Minerals Engineering 210 (2024) 108652

Contents lists available at ScienceDirect

Minerals Engineering

journal homepage: www.elsevier.com/locate/mineng

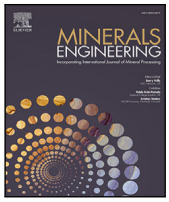

# Modelling, analysis and validation of a dynamic dense medium separation circuit model for detecting medium losses

C.S. Lowry [a,b], J.D. le Roux [b], I.K. Craig [b,*]

[a] Anglo American, Johannesburg, South Africa
[b] Department of Electrical, Electronic and Computer Engineering, University of Pretoria, Pretoria, South Africa

ARTICLE INFO

*Keywords:*
Dense medium separation
Extended Kalman filter
Modelling
Observability
Process control
Iron ore

ABSTRACT

Dense medium separation circuits use a dense medium to separate low density waste material from high density valuable minerals. Since the dense medium is an expensive consumable, it is recovered after separation of the valuable minerals from waste. A dynamic nonlinear model of a dense medium separation circuit of an iron ore plant in South Africa is developed to track the flow of medium in the circuit. An extended Kalman filter is designed for estimating observable but unmeasured states. The model is validated using online plant data. This paper serves as a precursor for further work to detect and mitigate expensive medium losses in the circuit.

## 1. Introduction

Dense medium separation (DMS) is a beneficiation process that separates valuable minerals from waste material, with the basic principle being the separation of low density material from high density material (Legault-Seguin et al., 2017). A dense medium is employed to achieve this separation. The medium is used in a separation vessel, and then recovered. In iron ore processing, ferrosilicon is used as the medium, which is an expensive consumable (Maré et al., 2015; Tom, 2015; Scott, 2017). Medium losses can contribute between 18% and 39% of the total operating costs of metalliferous DMS plants (Rayner and Napier-Munn, 2003b; Dardis, 1989). Therefore, the aim of this paper is to develop a dynamic mathematical model of a DMS plant that can aid in identifying and reducing medium losses to improve the economic performance of the plant.

Fig. 1 illustrates a dense medium separation circuit. Correctly sized ore is fed to a dense medium cyclone, where higher density valuable material forms the underflow of the cyclone, and lower density waste material forms the overflow (Napier-Munn, 2018). The overflow from the cyclone is sent to a drain-and-rinse screen. The medium slurry is drained from the waste material and sent to the correct medium tank. The remaining waste in the screen is then rinsed, with the rinsed medium reporting to the dilute medium tank. The waste in the overflow of the screen is transported via conveyor belts to the tailings. The underflow from the cyclone is also sent to a drain-and-rinse screen. The medium slurry is drained from the waste material and sent to the correct medium tank. The remaining material in the screen is rinsed with wash water. The rinsed medium slurry is sent to the dilute medium tank. The valuable material in the overflow from the screen is transported via conveyor belts to product stockpiles (Legault-Seguin et al., 2017).

The medium recovery circuit consists of a correct medium tank, a secondary tank, a dilute medium tank, two densifiers (primary and secondary), and the magnetic separator. The medium slurry is sent from the correct medium tank to either the mixing box, or to a primary cyclone densifier. The underflow of the primary cyclone densifier returns to the correct medium tank while the overflow is sent to the secondary tank. The secondary tank feeds a secondary pipe densifier, where the overflow passes to the dilute medium tank and the underflow passes to the correct medium tank. Finally, the slurry in the dilute medium tank can be diluted further with water before it is pumped to a magnetic separator. The effluent from the magnetic separator is sent to a degrit circuit, and the concentrate is returned to the correct medium tank.

Medium can be lost at the drain-and-rinse screens either due to adhesion to the ore or due to screen-blinding. Medium can also be lost in the effluent of the magnetic separator, or at the mixing box when blockages cause an overflow (Dardis, 1989; Napier-Munn et al., 1995).

An accurate model of the DMS circuit can assist to identify excessive medium losses. Using the principle of the conservation of mass, Meyer and Craig (2010) modelled the DMS circuit of a coal plant as individual units. The fundamental difference between a coal DMS circuit and an iron ore DMS circuit is that in an iron ore circuit, the product is denser and therefore reports to the underflow of the dense medium cyclone, while the waste reports to the overflow. This is the opposite in a coal DMS circuit. Meyer and Craig (2010) modelled both ore and medium

* Corresponding author.
*E-mail address:* ian.craig@up.ac.za (I.K. Craig).

https://doi.org/10.1016/j.mineng.2024.108652
Received 10 November 2023; Received in revised form 4 March 2024; Accepted 5 March 2024
Available online 16 March 2024

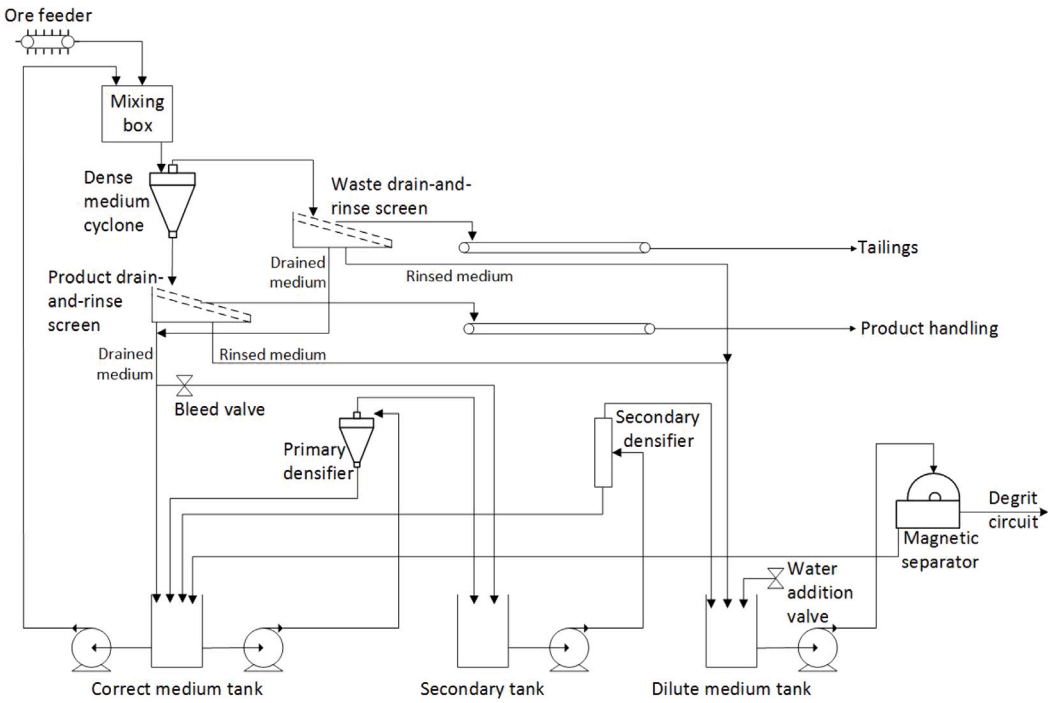


**Fig. 1.** Diagram of a dense medium separation circuit at an iron ore plant in South Africa.

flows of the specified units with a view to enable development of dynamic control of the yield and grade of the product.

The contribution of this paper is a dynamic nonlinear model of the iron ore DMS circuit in Fig. 1 (which, in addition to the mixing box, dense medium cyclone, and correct medium tank, which were modelled by Meyer and Craig (2010), also includes the product and waste drain-and-rinse screens, the secondary and dilute medium tanks, the primary and secondary densifiers, and the magnetic separator). The model described in this paper specifically focuses on the flow of medium in the circuit, and only includes the flow of ore in units where it affects the flow of medium. This means that the model developed herein does not give insight into the yield and grade of the product, but rather focuses on medium flows within the entire circuit, for the purposes of allowing for medium loss detection.

This model is developed in Section 2. Not all plant model parameters are known and not all input and output variables are measured, and so the developed model is analysed for observability in Section 3. If model states and parameters are unknown but observable as shown in Section 3, these states and parameters can theoretically be estimated using state estimation. In Section 4, state estimation using the extended Kalman filter is applied to online plant data from a DMS circuit for an iron ore plant in South Africa during a mixing box blockage event, which can lead to medium losses. Conclusions and recommendations are provided in Section 5.

## 2. Model development

This section presents the unit process models for the DMS circuit in Fig. 1. The model elements are presented in state-space as:

$$\begin{aligned} \dot{\boldsymbol{x}} &= f(t, \boldsymbol{x}, \boldsymbol{u}, \boldsymbol{d}) \\ \boldsymbol{y} &= g(t, \boldsymbol{x}, \boldsymbol{u}, \boldsymbol{d}), \end{aligned} \tag{1}$$

where $\boldsymbol{x} \in \mathfrak{R}^{n_x}$, $\boldsymbol{u} \in \mathfrak{R}^{n_u}$, $\boldsymbol{d} \in \mathfrak{R}^{n_d}$ and $\boldsymbol{y} \in \mathfrak{R}^{n_y}$ are the model states, inputs, process disturbances and measured outputs respectively.

For the circuit tanks, which do not receive ore but rather only medium (and water in the case of the dilute medium tank), only medium flows (and water where applicable) are modelled. The same is true of the primary and secondary densifiers, and the magnetic separator. The mixing box, which receives both ore and medium, is modelled considering both ore and medium. The dense medium cyclone and drain-and-rinse screens are combined into a simplified unit, and only the flow of medium is considered, as the ore from this simplified unit exits the circuit via the product and waste conveyors, and therefore its effect on the flow of medium in the rest of the circuit (which is the focus of this paper) is considered negligible.

### 2.1. Pump models

For the circuit tank models, a general model for the pumps used in the circuit shown in Fig. 1 is required. For each pump, the flow rate is not measured and only the pump speed is known. Furthermore, for this work, the principle of the conservation of volume is used. It is assumed that the material flows are similar to liquids and consequently incompressible. The pump speed, discharge flowrate and discharge pressure are measured variables. Only the hydraulic part of the pump is modelled (Ghafouri et al., 2012).

The pump characteristic curves, provided by the pump manufacturers, gives an indication of the relationship between the total dynamic head, and the volumetric flow rate produced by a pump, at a specific speed. Fig. 2 gives an example of the characteristic curve for a pump with a maximum speed of 805 rpm.

The curves in Fig. 2 can be fitted to a quadratic function over normal operating ranges for a specific pump speed. Furthermore, according to the pump affinity laws, the head developed by a pump at zero flow rate is proportional to the square of the speed of the pump (Karassik, 2008). The respective curves at all speeds can be constructed as follows:

$$H_p = H_{max} n^2 - SQ^2, \tag{2}$$

where $H_{max}$ [m] is the maximum head when there is no flow and the pump is at maximum speed, $n$ is the ratio of the current speed to the maximum speed of the pump, $S$ [$s^2/m^5$] is the curve parameter obtained from the pump curves, and $Q$ [$m^3/s$] is the volumetric flow rate of slurry.

Bernoulli's equation (Karassik, 2008) which asserts that the combination of pressure and the sum of kinetic and potential energy is

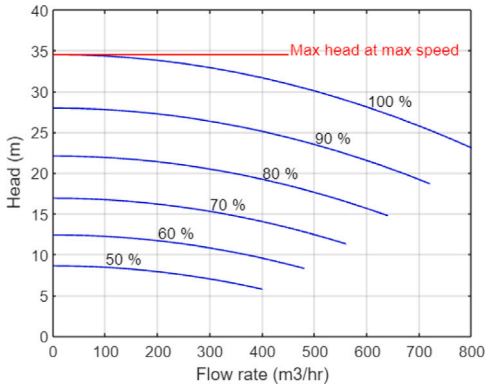


**Fig. 2.** Characteristic pump curves for correct medium pump (adapted from Minerals (2012)). The curves are given as percentages of the maximum speed.

**Table 1**
Correct medium tank model variables.

| Variable | Unit | Description |
|---|---|---|
| Measured at the plant | | |
| $h_{lev(CM)}$ | m | Correct medium tank level |
| $P_{PD}$ | kPa | Primary densifier pump pressure |
| $n_{CM}$ | – | Correct medium pump speed fraction |
| $n_{PD}$ | – | Primary densifier pump speed fraction |
| $\rho_{CM}$ | t/m$^3$ | Density of slurry in correct medium tank |
| Not measured at the plant | | |
| $Q_{CM}$ | m$^3$/s | Correct medium pump flow rate |
| $Q_{PD}$ | m$^3$/s | Primary densifier pump flow rate |
| $P_{CM}$ | kPa | Correct medium pump pressure |
| $Q_{in(CM)}$ | m$^3$/s | Flow into correct medium tank |

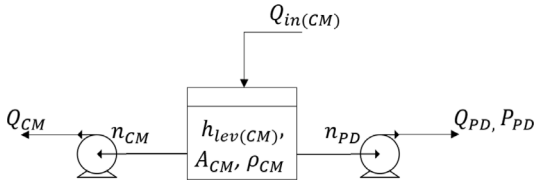


**Fig. 3.** Correct medium tank unit, with primary densifier pump and correct medium pump.

constant over time. Therefore, the total head developed by a pump at a specific speed is defined as:

$$H_{max}n^2 = \frac{P}{\rho g} + \frac{Q^2}{2gA^2} + h, \tag{3}$$

where $P$ [kPa] is the pump discharge pressure, $\rho$ [t/m$^3$] is the density of the pumped slurry, $g$ [m/s$^2$] is the gravitational acceleration constant, $A$ [m$^2$] is the cross-sectional area of the discharge pipe, and $h$ [m] is the total static head. The terms $\frac{P}{\rho g}$ and $h$ in (3) are collapsed into the $H_p$ term in (2), while $\frac{1}{2gA^2}$ in (3) is equivalent to $S$ in (2).

From (3), the discharge pressure can be written as:

$$P = \rho g\left(H_{max}n^2 - \frac{Q^2}{2gA^2} - h\right), \tag{4}$$

where the static head $h = h_{dis} - h_{lev}$ can be expressed in terms of the height to which the slurry is pumped ($h_{dis}$ [m]) and the height of slurry in the tank ($h_{lev}$ [m]).

### 2.2. Correct medium tank

The correct medium tank in Fig. 1 is redrawn in Fig. 3. Table 1 describes the process variables for the correct medium tank in terms of measured and unmeasured variables, where subscript CM refers to the correct medium and PD refers to the primary densifier. The dynamics of the level of the correct medium tank can be obtained using the principle of the conservation of volume. Therefore:

$$\frac{dh_{lev(CM)}}{dt} = \frac{1}{A_{CM}}\left(Q_{in(CM)} - Q_{CM} - Q_{PD}\right), \tag{5}$$

where $Q_{CM}$ [m$^3$/s] and $Q_{PD}$ [m$^3$/s] are the discharge volumetric flow rates of the correct medium pump and the primary densifier pump respectively, $Q_{in(CM)}$ [m$^3$/s] is the sum of the volumetric flow of medium returned to the correct medium tank, and $A_{CM}$ [m$^2$] is the cross-sectional area of the correct medium tank. These discharge volumetric flow rates are phenomenologically modelled according to Newton's second law of motion applied to fluids (Versteeg and Malalasekera, 2007):

$$\begin{aligned} k_{j(CM)}\frac{dQ_{CM}}{dt} &= -k_pQ_{CM}^2 + \rho_{CM}gH_{p(CM)} \\ &\quad - \rho_{CM}g\left(h_{dis(CM)} - h_{lev(CM)}\right) \end{aligned} \tag{6}$$

$$\begin{aligned} k_{j(PD)}\frac{dQ_{PD}}{dt} &= -k_pQ_{PD}^2 + \rho_{CM}gH_{p(PD)} \\ &\quad - \rho_{CM}g\left(h_{dis(PD)} - h_{lev(PD)}\right), \end{aligned} \tag{7}$$

where $\rho_{CM}$ [t/m$^3$] is the density of the slurry in the correct medium tank, $k_p$ is the resistance coefficient of the pipe, $k_{j(CM)}$ [t m$^2$] and $k_{j(PD)}$ [t m$^2$] are the inertia of the fluid for the correct medium tank and primary densifier respectively (Kallesoe et al., 2006), and $H_{p(CM)}$ [m] and $H_{p(PD)}$ [m] are given by (2).

A state-space model of the correct medium tank is:

$$\begin{aligned} \dot{\boldsymbol{x}}_{CM} &= f_{CM}(t, \boldsymbol{x}_{CM}, \boldsymbol{u}_{CM}, \boldsymbol{d}_{CM}) \\ &= \begin{bmatrix} \frac{1}{A_{CM}}\left(Q_{in(CM)} - Q_{CM} - Q_{PD}\right) \\ \frac{1}{k_{j(CM)}}\left(\rho_{CM}g(H_{p(CM)} - h_{CM}) - k_pQ_{CM}^2\right) \\ \frac{1}{k_{j(PD)}}\left(\rho_{CM}g(H_{p(PD)} - h_{PD}) - k_pQ_{PD}^2\right) \end{bmatrix} \end{aligned} \tag{8}$$

$$\begin{aligned} \boldsymbol{y}_{CM} &= g_{CM}(t, \boldsymbol{x}_{CM}, \boldsymbol{u}_{CM}, \boldsymbol{d}_{CM}) \\ &= \begin{bmatrix} h_{lev(CM)} \\ \rho_{CM}g\left(H_{max(PD)}n_{PD}^2 - \frac{Q_{PD}^2}{2A_{PD}^2g} - h_{PD}\right) \\ \rho_{CM} \end{bmatrix}, \end{aligned} \tag{9}$$

where $h_{CM} = h_{dis(CM)} - h_{lev(CM)}$ and $h_{PD} = h_{dis(PD)} - h_{lev(CM)}$. The model states, inputs, disturbances, and measured variables are given by $\boldsymbol{x}_{CM} = \left[h_{lev(CM)}, Q_{CM}, Q_{PD}\right]^T$, $\boldsymbol{u}_{CM} = \left[n_{CM}, n_{PD}\right]^T$, $\boldsymbol{d}_{CM} = \left[\rho_{CM}, Q_{in(CM)}\right]^T$, and $\boldsymbol{y}_{CM} = \left[h_{lev(CM)}, P_{PD}, \rho_{CM}\right]^T$. respectively. Note that $Q_{in(CM)}$ is not measured and is included as a process disturbance. Similarly, $\rho_{CM}$ is measured, and is treated as a known but uncontrolled disturbance.

Table 2 shows the values of the parameters required for the model. Parameters $H_{max(CM)}$, $H_{max(PD)}$, $S_{CM}$, and $S_{PD}$ are obtained from the pump curve provided by the manufacturer. Parameters $k_{j(CM)}$ and $k_{j(PD)}$ are functions of $\rho_{CM}$, as well as the length and cross-sectional area of the correct medium pump and primary densifier pipes respectively.

### 2.3. Secondary tank model

The secondary tank shown in Fig. 1 is redrawn in Fig. 4. It can be modelled similarly to the correct medium tank. The model is in fact simpler, as the secondary tank has only one pump extracting slurry to pump it to the secondary densifier. Table 3 describes the process variables for the secondary tank in terms of measured and unmeasured variables, where subscript SD refers to the secondary densifier.

A state-space model of the secondary tank is:

$$\dot{\boldsymbol{x}}_{sec} = f_{sec}(t, \boldsymbol{x}_{sec}, \boldsymbol{u}_{sec}, \boldsymbol{d}_{sec}) \tag{10}$$

**Table 2**
Correct medium tank model parameters.

| Variable | Value | Description |
|---|---|---|
| $H_{max(CM)}$ | 34.5 m | Maximum head of correct medium pump |
| $H_{max(PD)}$ | 17 m | Maximum head of primary densifier pump |
| $S_{CM}$ | 0.072 $s^2/m^5$ | Quadratic term of correct medium pump curve |
| $S_{PD}$ | 0.2 $s^2/m^5$ | Quadratic term of primary densifier pump curve |
| $k_{j(CM)}$ | 961 t $m^2$ | Hydraulic inertia of fluid for correct medium pump |
| $k_{j(PD)}$ | 721 t $m^2$ | Hydraulic inertia of fluid for primary densifier pump |
| $A_{CM}$ | 8 $m^2$ | Cross-sectional area of correct medium tank |
| $A_{PD}$ | 0.011 $m^2$ | Area of primary densifier pump pipe |
| $k_p$ | 140 | Resistance coefficient of pipe (steel) |
| $h_{dis(CM)}$ | 10.83 m | Height slurry is pumped to by correct medium pump |
| $h_{dis(PD)}$ | 4.5 m | Height slurry is pumped to by primary densifier pump |

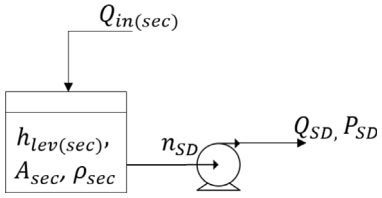


**Fig. 4.** Secondary tank unit.

**Table 3**
Secondary tank model variables.

| Variable | Unit | Description |
|---|---|---|
| Measured at the plant | | |
| $h_{lev(sec)}$ | m | Secondary tank level |
| $P_{SD}$ | kPa | Secondary densifier pump pressure |
| $n_{SD}$ | – | Secondary densifier pump speed fraction |
| $\rho_{sec}$ | t/$m^3$ | Density of slurry in secondary tank |
| Not measured at the plant | | |
| $Q_{SD}$ | $m^3/s$ | Secondary densifier pump flow rate |
| $Q_{in(sec)}$ | $m^3/s$ | Flow into secondary tank |

$$= \begin{bmatrix} \frac{1}{A_{sec}} \left( Q_{in(sec)} - Q_{SD} \right) \\ \frac{1}{k_{j(SD)}} \left( \rho_{sec} g (H_{p(SD)} - h_{SD}) - k_p Q_{SD}^2 \right) \end{bmatrix}$$

$$\boldsymbol{y}_{sec} = g_{sec}(t, \boldsymbol{x}_{sec}, \boldsymbol{u}_{sec}, \boldsymbol{d}_{sec}) \tag{11}$$
$$= \begin{bmatrix} h_{lev(sec)} \\ \rho_{sec} g \left( H_{max(SD)} n_{SD}^2 - \frac{Q_{SD}^2}{2 A_{SD}^2 g} - h_{SD} \right) \\ \rho_{sec} \end{bmatrix},$$

where $h_{SD} = h_{dis(SD)} - h_{lev(sec)}$. The model states, inputs, disturbances and measured variables are given by $\boldsymbol{x}_{sec} = \left[ h_{lev(sec)}, Q_{SD} \right]^T$, $\boldsymbol{u}_{sec} = n_{SD}$, $\boldsymbol{d}_{sec} = \left[ \rho_{sec}, Q_{in(sec)} \right]^T$, and $\boldsymbol{y}_{sec} = \left[ h_{lev(sec)}, P_{SD}, \rho_{sec} \right]^T$ respectively. Note that the total flow into the secondary tank, $Q_{in(sec)}$, consists of the overflow from the primary densifier, as well as a small bleed stream of drained medium from the drain-and-rinse screens. Since these streams are not measured, $Q_{in(sec)}$ is modelled as a process disturbance. Similarly, $\rho_{sec}$ is measured, and is treated as a known but uncontrolled disturbance. Table 4 shows the values of the parameters for the model.

### 2.4. Dilute medium tank

The dilute medium tank in Fig. 1 is redrawn in Fig. 5. The model differs from the secondary tank model, as the discharge pressure of the dilute medium tank is not measured. Furthermore, water is added to the dilute medium tank via a control valve, which is controlled by a level control PID. Table 5 describes the process variables for the dilute medium tank in terms of measured and unmeasured variables, where subscript DM refers to the dilute medium tank.

**Table 4**
Secondary tank model parameters.

| Variable | Value | Description |
|---|---|---|
| $H_{max(SD)}$ | 32.1 m | Maximum head of secondary densifier pump |
| $S_{SD}$ | 0.324 $s^2/m^5$ | Quadratic term of secondary densifier pump curve |
| $k_{j(SD)}$ | 721 t $m^2$ | Hydraulic inertia of fluid for secondary densifier pump |
| $A_{sec}$ | 2.73 $m^2$ | Cross-sectional area of secondary tank |
| $A_{SD}$ | 0.011 $m^2$ | Area of secondary densifier pump pipe |
| $k_p$ | 140 | Resistance coefficient of steel pipe |
| $h_{dis(SD)}$ | 11 m | Height slurry is pumped to by secondary densifier pump |

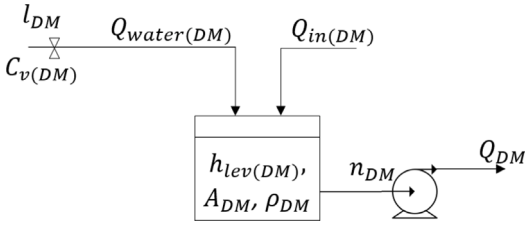


**Fig. 5.** Dilute medium tank unit.

**Table 5**
Dilute medium tank model variables.

| Variable | Unit | Description |
|---|---|---|
| Measured at the plant | | |
| $h_{lev(DM)}$ | m | Dilute medium tank level |
| $n_{DM}$ | – | Dilute medium pump speed fraction |
| $l_{DM}$ | – | Water valve opening |
| Not measured at the plant | | |
| $Q_{DM}$ | $m^3/s$ | Dilute medium pump flow rate |
| $P_{DM}$ | kPa | Dilute medium pump pressure |
| $Q_{water(DM)}$ | $m^3/s$ | Water addition to dilute medium tank |
| $Q_{in(DM)}$ | $m^3/s$ | Flow into dilute medium tank |
| $\rho_{DM}$ | t/$m^3$ | Density of slurry in dilute medium tank |

The flow rate of water through the control valve ($Q_{water(DM)}$ [$m^3/s$]) is modelled as:

$$Q_{water(DM)} = C_v f(l_{DM}) \sqrt{\frac{\Delta P_v}{g_s}} \tag{12}$$

where $C_v$ [$m^3/s$] is the valve size coefficient supplied by manufacturers, $\Delta P_v$ [kPa] is the pressure drop across the valve, $g_s$ is the liquid specific gravity of the fluid, and $l_{DM}$ is the fraction opening of the valve bound between 0 (fully closed) and 1 (fully opened). The function $f(l_{DM})$ is dependent on the control valve characteristic curve, that is, if it is fast opening, linear or equal percentage (Seborg et al., 2016). For this work, it is assumed that the pressure drop across the valve, $\Delta P_v$ is constant, while the specific gravity $g_s$ is known to be constant (and equal to 1). Therefore, the $\sqrt{\frac{\Delta P_v}{g_s}}$ term is therefore absorbed with the coefficient $C_{v(DM)}$ into coefficient $k_v$. Furthermore, the valve is assumed to be linear. Therefore Eq. (12) is simplified as:

$$Q_{water(DM)} = k_v l_{DM} \tag{13}$$

A state-space model of the dilute medium tank is:

$$\dot{\boldsymbol{x}}_{DM} = f_{DM}(t, \boldsymbol{x}_{DM}, \boldsymbol{u}_{DM}) \tag{14}$$
$$= \begin{bmatrix} \frac{1}{A_{DM}} \left( Q_{in(DM)} - Q_{DM} + k_v l_{DM} \right) \\ \frac{1}{k_{j(DM)}} \left( \rho_{DM} g (H_{p(DM)} - h_{DM}) - k_p Q_{DM}^2 \right) \end{bmatrix}$$

$$\boldsymbol{y}_{DM} = g_{DM}(t, \boldsymbol{x}_{DM}, \boldsymbol{u}_{DM}) \tag{15}$$
$$= h_{lev(DM)},$$

where $h_{DM} = h_{dis(DM)} - h_{lev(DM)}$. The model states, input, disturbances and outputs are given by $\boldsymbol{x}_{DM} = \left[ h_{lev(DM)}, Q_{DM} \right]^T$, $\boldsymbol{u}_{DM} =$

**Table 6**
Dilute medium tank model parameters.

| Variable | Value | Description |
|---|---|---|
| $H_{max(DM)}$ | 5.14 m | Maximum head of dilute medium pump |
| $S_{DM}$ | 0.36 $s^2/m^5$ | Quadratic term of dilute medium pump curve |
| $k_{j(DM)}$ | 481 t $m^2$ | Hydraulic inertia of fluid for dilute medium pump |
| $A_{DM}$ | 4.13 $m^2$ | Cross-sectional area of dilute medium tank |
| $k_p$ | 140 | Resistance coefficient of pipe (steel) |
| $h_{dis(DM)}$ | 3.4 m | Height slurry is pumped to by dilute medium pump |

$[n_{DM}, l_{DM}]^T$, $\boldsymbol{d}_{DM} = [\rho_{DM}, Q_{in(DM)}]^T$, and $\boldsymbol{y}_{DM} = h_{lev(DM)}$. The unmeasured variables, $Q_{in(DM)}$ and $\rho_{DM}$, are modelled as process disturbances. Table 6 shows the values of the parameters for the model.

### 2.5. Mixing box

The mixing box receives both ore from the feeder and medium from the correct medium pump, as can be seen in Fig. 1. The mixing box is elevated above the dense medium cyclone, which is either gravity-fed from the mixing box (as in the case of this circuit), or pump-fed. The mixing box is modelled as a gravity-drained tank, and the conservation of volume is used to model the level:

$$A_{MB}\frac{dh_{lev(MB)}}{dt} = Q_{CM} + Q_{ore,in(MB)} - Q_{out(MB)}, \tag{16}$$

where $Q_{CM}$ [$m^3$/s] and $Q_{ore,in(MB)}$ [$m^3$/s] are the volumetric flow rates of the medium and ore entering the mixing box respectively, $Q_{out(MB)}$ [$m^3$/s] is the volumetric flow rate of the mixture of ore and medium draining out of the mixing box by gravity, and $h_{lev(MB)}$ [m] is the height of slurry in the mixing box. Note that the material in the mixing box is assumed well-mixed. Therefore the ratio of medium to ore in the flow out of the mixing box is considered equal to that of the flow in (by ignoring any hold-up in the mixing box). The flow of the mixture gravity-draining out can be modelled as follows (Jang, 2016):

$$Q_{out(MB)} = k_{MB}\sqrt{h_{lev(MB)}}, \tag{17}$$

$k_{MB}$ [$m^{5/2}$/s] is a function of the mixing box opening geometry, and it is a constant. It can, however, be used to model disturbances, such as a blockage in the mixing box which occurs frequently. Blockages cause overflows of the mixing box which lead to the loss of medium.

The level of the mixing box is measured, however, the reading is notoriously unreliable at the plant in question due to the geometry of the mixing box, as well as the nature of the environment: the medium entering the mixing box causes significant splashes that interfere with the instrument. Therefore, the mixing box level is considered unmeasured. The feed pressure to the dense medium cyclone is measured, and this is a function of the difference in height between the dense medium cyclone and the slurry level in the mixing box. The pressure, $P_{MB}$ [kPa], can be calculated as follows:

$$P_{MB} = \rho_{MB} g(H_{MB} + h_{lev(MB)}), \tag{18}$$

where $\rho_{MB}$ [t/$m^3$] is the density of the ore and medium mixture in the mixing box, and $H_{MB}$ [m] is the height differential between the mixing box outlet and the pressure gauge.

Fig. 6 illustrates the mixing box. Table 7 describes the process variables for the mixing box in terms of measured and unmeasured variables, where subscript MB refers to the mixing box.

Note that while $Q_{CM}$ is not directly measured, it is available via state estimation of the correct medium tank system. Additionally, $\rho_{MB}$ is not measured, but can be calculated using the ratio of ore to medium in the feed, as well as the known bulk density of the ore, $\rho_{ore}$, and the measured density of the correct medium being pumped from the correct medium tank, $\rho_{CM}$, as follows (by ignoring any hold-up in the mixing box):

$$\rho_{MB} = \frac{Q_{CM}\rho_{CM} + Q_{ore,in(MB)}\rho_{ore}}{Q_{CM} + Q_{ore,in(MB)}}, \tag{19}$$

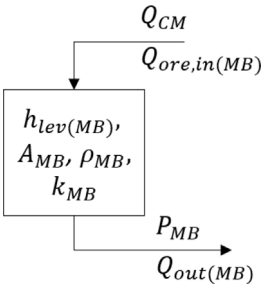


**Fig. 6.** Mixing box unit.

**Table 7**
Mixing box tank model variables.

| Variable | Unit | Description |
|---|---|---|
| Measured at the plant | | |
| $Q_{ore,in(MB)}$ | $m^3$/s | Ore flow to mixing box |
| $P_{MB}$ | kPa | Mixing box discharge pressure |
| $\rho_{MB}$ | t/$m^3$ | Density of slurry in mixing box |
| Not measured at the plant | | |
| $h_{lev(MB)}$ | m | Mixing box level |
| $Q_{out(MB)}$ | $m^3$/s | Flow rate out of mixing box |

**Table 8**
Mixing box model parameters.

| Variable | Value | Description |
|---|---|---|
| $A_{MB}$ | 0.429 $m^2$ | Cross-sectional area of mixing box |
| $H_{MB}$ | 5.7 m | Height differential of mixing box outlet |
| $k_{MB}$ | Unknown | Mixing box outlet coefficient |

A state-space model of the mixing box is:

$$\begin{aligned}\dot{\boldsymbol{x}}_{MB} &= f_{MB}(t, \boldsymbol{x}_{MB}, \boldsymbol{u}_{MB}, \boldsymbol{d}_{MB}) \\ &= \frac{Q_{CM} + Q_{ore,in(MB)} - k_{MB}\sqrt{h_{lev(MB)}}}{A_{MB}}\end{aligned} \tag{20}$$

$$\begin{aligned}\boldsymbol{y}_{MB} &= g_{MB}(t, \boldsymbol{x}_{MB}, \boldsymbol{u}_{MB}, \boldsymbol{d}_{MB}) \\ &= \begin{bmatrix}\rho_{MB} g(H_{MB} + h_{lev(MB)}) \\ \rho_{MB} \\ Q_{CM}\end{bmatrix},\end{aligned} \tag{21}$$

where the model states, inputs, disturbances and outputs are given by $\boldsymbol{x}_{MB} = h_{lev(MB)}$, $\boldsymbol{u}_{MB} = Q_{ore,in(MB)}$, $\boldsymbol{d}_{MB} = [\rho_{MB}, Q_{CM}]^T$, and $\boldsymbol{y}_{MB} = [P_{MB}, \rho_{MB}, Q_{CM}]^T$ respectively.

### 2.6. Uninstrumented units

The primary and secondary densifiers, the magnetic separator, the dense medium cyclone, and the product and waste drain-and-rinse screens are not instrumented in the plant. Details of the steady-state models developed for these units can be found in Appendix. The models are sufficient for an off-line simulation of the plant, whether for operator training or controller testing purposes.

## 3. Observability analysis

The dense medium separation circuit, seen in Fig. 1, is analysed for observability. The analysis is done to determine if the level of instrumentation is theoretically sufficient for identifying medium losses. If model states and parameters are unknown but observable as shown in this section, these states and parameters can theoretically be estimated using e.g. an EKF, as is shown in Section 4.

### 3.1. Observability theory

For the observability analysis, the unmeasured disturbances in the unit process models above can be included in an observer by including the unmeasured disturbances as constant states in the state–vector in (1). The augmented system is:

$$\begin{aligned} \dot{\boldsymbol{z}} &= \begin{bmatrix} \dot{\boldsymbol{x}} \\ \dot{\boldsymbol{d}} \end{bmatrix} = \begin{bmatrix} f(t,\boldsymbol{z},\boldsymbol{u}) \\ 0 \end{bmatrix} \\ \boldsymbol{y} &= g(t,\boldsymbol{z},\boldsymbol{u}), \end{aligned} \tag{22}$$

where $\boldsymbol{z} \in \Re^n$ and $n = n_x + n_d$.

The model in (22) can be linearized around an equilibrium point using a small signal approach (Seborg et al., 2016). For small deviations around an equilibrium point $(\boldsymbol{z}_q, \boldsymbol{u}_q)$ where $\dot{\boldsymbol{z}} = 0$, the linearized system can be written as:

$$\begin{aligned} \delta\dot{\boldsymbol{z}} &= A\delta\boldsymbol{z} + B\delta\boldsymbol{u} \\ \delta\boldsymbol{y} &= C\delta\boldsymbol{z} + D\delta\boldsymbol{u}, \end{aligned} \tag{23}$$

where

$$A = \frac{\partial}{\partial \boldsymbol{z}} f(t,\boldsymbol{z},\boldsymbol{u})|_{(\boldsymbol{z}_q,\boldsymbol{u}_q)},\ B = \frac{\partial}{\partial \boldsymbol{u}} f(t,\boldsymbol{z},\boldsymbol{u})|_{(\boldsymbol{z}_q,\boldsymbol{u}_q)},$$
$$C = \frac{\partial}{\partial \boldsymbol{z}} g(t,\boldsymbol{z},\boldsymbol{u})|_{(\boldsymbol{z}_q,\boldsymbol{u}_q)},\ \text{and}\ D = \frac{\partial}{\partial \boldsymbol{u}} g(t,\boldsymbol{z},\boldsymbol{u})|_{(\boldsymbol{z}_q,\boldsymbol{u}_q)}.$$

The deviation variables are defined as $\delta\boldsymbol{z} = \boldsymbol{z} - \boldsymbol{z}_q$ and $\delta\boldsymbol{u} = \boldsymbol{u} - \boldsymbol{u}_q$.

The dynamical system (23) is state observable if and only if the observability matrix $\mathcal{O}$ has full column rank $n$, where (Skogestad and Postlethwaite, 2005):

$$\mathcal{O} = \left[C^T, A^T C^T, \ldots A^{T^{n-1}} C^T\right]^T. \tag{24}$$

### 3.2. Correct medium tank model observability

The correct medium tank nonlinear model in (8) and (9) is augmented such that $\boldsymbol{z}_{CM} = [\boldsymbol{x}_{CM}^T, \boldsymbol{d}_{CM}^T]^T$. The linearized model matrices (obtained using MATLAB's symbolic toolbox) as per (23) are given below after substitution of the known parameter values in Table 2:

$$\boldsymbol{A}_{CM} = \begin{bmatrix} 0 & -0.125 & -0.125 & 0 & 0.125 \\ 0.0102\rho_{CM} & a_{22(CM)} & 0 & a_{24(CM)} & 0 \\ 0.0136\rho_{CM} & a_{32(CM)} & -280Q_{PD} & a_{34(CM)} & 0 \\ 0 & 0 & 0 & 0 & 0 \\ 0 & 0 & 0 & 0 & 0 \end{bmatrix}$$

$$\boldsymbol{B}_{CM} = \begin{bmatrix} 0 & 0 \\ 0.704 n_{CM}\rho_{CM} & 0 \\ 0.939 n_{CM}\rho_{CM} & 0 \\ 0 & 0 \\ 0 & 0 \end{bmatrix}$$

$$\boldsymbol{C}_{CM} = \begin{bmatrix} 1 & 0 & 0 & 0 & 0 \\ 9.81\rho_{CM} & 0 & -31.85 Q_{PD}\rho_{CM} & c_{24(CM)} & 0 \\ 0 & 0 & 0 & 1 & 0 \end{bmatrix},$$

where:

$$\begin{aligned} a_{22(CM)} &= -280 Q_{CM} - 4.08\times10^{-7} Q_{CM}\rho_{CM} \\ a_{24(CM)} &= -2.04\times10^{-7} Q_{CM}^2 + 0.352 n_{CM}^2 \\ &\quad + 0.0102 h_{lev(CM)} - 0.213 \\ a_{32(CM)} &= -5.44\times10^{-7} Q_{CM}\rho_{CM} \\ a_{34(CM)} &= -2.72\times10^{-7} Q_{CM}^2 + 0.469 n_{CM}^2 \\ &\quad + 0.0136 h_{lev(CM)} - 0.283 \\ c_{24(CM)} &= -15.92 Q_{PD}^2 + 122.6 n_{PD}^2 + 9.81 h_{lev(CM)} - 111. \end{aligned}$$

The observability matrix $\mathcal{O}_{CM}$ as determined from (24) has a full rank of 5, i.e., all states and parameters are observable. The determinant of the first five rows and columns of the matrix:

$$\det\left(\mathcal{O}_{CM5\times5}\right) = 6.9\times10^5 Q_{CM} Q_{PD}^2 \rho_{CM}^3$$

will only be zero if $Q_{CM}$ $Q_{PD}$, or $\rho_{CM}$ is zero. Therefore, the system is expected to be observable for normal operating conditions.

### 3.3. Secondary tank model observability

The secondary tank model in (10) and (11) is augmented such that $\boldsymbol{z}_{sec} = [\boldsymbol{x}_{sec}^T, \boldsymbol{d}_{sec}]^T$. The linearized model matrices as per (23) are given below after substitution of the known parameter values in Table 4:

$$\boldsymbol{A}_{sec} = \begin{bmatrix} 0 & -0.366 & 0 & 0.366 \\ 0.0136\,\rho_{sec} & a_{22(sec)} & a_{23(sec)} & 0 \\ 0 & 0 & 0 & 0 \\ 0 & 0 & 0 & 0 \end{bmatrix}$$

$$\boldsymbol{B}_{sec} = \begin{bmatrix} 0 \\ 0.874\, n_{SD}\,\rho_{sec} \\ 0 \\ 0 \end{bmatrix}$$

$$\boldsymbol{C}_{sec} = \begin{bmatrix} 1 & 0 & 0 & 0 \\ 9.81\,\rho_{sec} & -31.8\, Q_{SD}\,\rho_{sec} & c_{23(sec)} & 0 \\ 0 & 0 & 1 & 0 \end{bmatrix},$$

where:

$$\begin{aligned} a_{22(sec)} &= -280\, Q_{SD} - 2.45\times10^{-6}\, Q_{SD}\,\rho_{sec} \\ a_{23(sec)} &= -1.22\times10^{-6}\, {Q_{SD}}^2 + 0.437\, {n_{SD}}^2 \\ &\quad + 0.0136\, h_{lev(sec)} - 0.265 \\ c_{23(sec)} &= -15.9\, {Q_{SD}}^2 + 315\, {n_{SD}}^2 + 9.81\, h_{lev(sec)} - 191. \end{aligned}$$

The observability matrix $\mathcal{O}_{sec}$ as determined from (24) has a full rank of 4, i.e., all states and parameters are observable. The determinant of the first four rows and columns of the matrix:

$$\det\left(\mathcal{O}_{sec4\times4}\right) = -11.7\, Q_{SD}\,\rho_{sec}$$

will only be zero if $Q_{SD}$ or $\rho_{sec}$ is zero. Therefore, the system is expected to be observable for normal operating conditions.

### 3.4. Dilute medium tank model observability

The dilute medium tank model in (14) and (15) is augmented such that $\boldsymbol{z}_{DM} = [\boldsymbol{x}_{DM}^T, k_v, \boldsymbol{d}_{DM}^T]^T$. The linearized model matrices as per (23) are given below after substitution of the known parameter values in Table 6:

$$\boldsymbol{A}_{DM} = \begin{bmatrix} 0 & -0.24 & 0.24\, l_{DM} & 0 & 0.24 \\ 0.02\,\rho_{DM} & a_{22(DM)} & 0 & a_{24(DM)} & 0 \\ 0 & 0 & 0 & 0 & 0 \\ 0 & 0 & 0 & 0 & 0 \\ 0 & 0 & 0 & 0 & 0 \end{bmatrix}$$

$$\boldsymbol{B}_{DM} = \begin{bmatrix} 0 & 0.242\, k_v \\ 0.21\, n_{DM}\,\rho_{DM} & 0 \\ 0 & 0 \\ 0 & 0 \\ 0 & 0 \end{bmatrix}$$

$$\boldsymbol{C}_{DM} = \begin{bmatrix} 1 & 0 & 0 & 0 & 0 \end{bmatrix},$$

where:

$$a_{22(DM)} = -280.0\, Q_{DM} - 4.08\times10^{-6}\, Q_{DM}\,\rho_{DM}$$

$$a_{24(DM)} = -2.04\times10^{-6}\,{Q_{DM}}^2 + 0.105\,{n_{DM}}^2 + 0.0204\,h_{lev(DM)} - 0.295.$$

The observability matrix $\mathcal{O}_{DM}$ as determined from (24) has a rank of 5. However, the determinant for any square part of the matrix is zero. Therefore, the system is not considered observable. The model is, therefore, further simplified by combining the flow rate of water into the tank from the dilute valve ($Q_{water}$) with the flow of medium into the tank $Q_{in(DM)}$ such that:

$$\dot{\boldsymbol{x}}_{DM} = f_{DM}(t, \boldsymbol{x}_{DM}, \boldsymbol{u}_{DM}) = \begin{bmatrix} \frac{1}{A_{DM}}\left(Q_{in(DM)} - Q_{DM}\right) \\ \frac{1}{k_{j(DM)}}\left(\rho_{DM}\, g (H_{p(DM)} - h_{DM}) - k_p Q_{DM}^2\right) \end{bmatrix} \tag{25}$$

$$\boldsymbol{y}_{DM} = g_{DM}(t, \boldsymbol{x}_{DM}, \boldsymbol{u}_{DM}) = h_{lev(DM)}, \tag{26}$$

with the model states, input, disturbances and outputs given by $\boldsymbol{x}_{DM} = \left[h_{lev(DM)}, Q_{DM}\right]^T$, $\boldsymbol{u}_{DM} = n_{DM}$, $\boldsymbol{d}_{DM} = \left[\rho_{DM}, Q_{in(DM)}\right]^T$, and $\boldsymbol{y}_{DM} = h_{lev(DM)}$. The unmeasured variables, $Q_{in(DM)}$ and $\rho_{DM}$, are modelled as process disturbances. Augmenting this model such that $\boldsymbol{z}_{DM} = [\boldsymbol{x}_{DM}^T, \boldsymbol{d}_{DM}^T]^T$, the resultant model has full rank of 4, ie., all states and parameters are observable. The determinant (which is too large to show), will only be zero if $Q_{DM}$ is zero. Therefore, the system is expected to be observable for normal operating conditions.

### 3.5. Mixing box model observability

The mixing box model in (20) and (21) is augmented such that $\boldsymbol{z}_{MB} = [\boldsymbol{x}_{MB}^T, k_{MB}, \boldsymbol{d}_{MB}^T]^T$. The linearized model matrices as per (23) are given below after substitution of the known parameter values in Table 8:

$$\boldsymbol{A}_{MB} = \begin{bmatrix} -\frac{1.17\,k_{MB}}{\sqrt{h_{lev(MB)}}} & -2.33\sqrt{h_{lev(MB)}} & 0 & 2.33 \\ 0 & 0 & 0 & 0 \\ 0 & 0 & 0 & 0 \\ 0 & 0 & 0 & 0 \end{bmatrix}$$

$$\boldsymbol{B}_{MB} = \begin{bmatrix} 2.33 \\ 0 \\ 0 \end{bmatrix}$$

$$\boldsymbol{C}_{MB} = \begin{bmatrix} 9.81\,\rho_{MB} & 0 & 9.81\,h_{lev(MB)} + 14.7 & 0 \\ 0 & 0 & 1 & 0 \\ 0 & 0 & 0 & 1 \end{bmatrix}.$$

The observability matrix $\mathcal{O}_{MB}$ as determined from (24) has a full rank of 4, i.e., all states and parameters are observable. The determinant

$$\det\left(\mathcal{O}_{MB3\times3}\right) = -224.0\sqrt{h_{lev(MB)}}\,{\rho_{MB}}^2$$

will only be zero if $h_{lev(MB)}$ or $\rho_{MB}$ is zero. Therefore, the system is expected to be observable for normal operating conditions.

## 4. State estimation using plant data

There are several sources of medium loss in the dense medium separation circuit. These sources of loss can be grouped into three categories: mixing box losses (due to overflows of the mixing box), drain-and-rinse screen losses (due to medium adhesion to the ore, or due to screen blinding which causes medium to run over the screens), and losses to the magnetic separator effluent (Dardis, 1989; Napier-Munn et al., 1995). The model developed in Section 2 can be used to simulate these sources of loss. Analysis of this simulation gives insight into how the key variables of the circuit are affected due to these loss scenarios, and the first order responses of these key variables to these simulated loss scenarios can be seen in Table 9.

**Table 9**
Table showing response of key circuit variables as a result of medium losses.

| | Mixing box blockage | Magnetic separator losses | Screen losses |
|---|---|---|---|
| $Q_{in(CM)}$ | ↘ | ↘ | ↘ |
| $Q_{in(sec)}$ | ↘ | — | — |
| $k_{MB}$ | ↘ | — | — |
| $h_{lev(MB)}$ | ↗ | — | — |

Plant data for a period when a blockage in the mixing box occurred are available. These data are used for state estimation. For all units, the data were sampled at a rate of $T_s = 5$ s.

### 4.1. Extended Kalman filter implementation

The observability analysis conducted in Section 3 indicates that the states for all the tanks in the circuit as well as the mixing box, are observable. A discrete time extended Kalman filter (EKF) is used as observer to estimate these states (Schneider and Georgakis, 2013; Simon, 2006).

The trapezoidal rule is used to discretize each nonlinear model in Section 2 as presented in continuous-time form by (22). The system and measurement equations are:

$$\begin{aligned} z_k &= f_{k-1}\left(z_{k-1}, u_{k-1}, w_{k-1}\right) \\ y_k &= g_k\left(z_k, u_k, v_k\right), \end{aligned} \tag{27}$$

where the process noise $w_k \sim (0, Q_k)$ is white noise with covariance $Q_k > 0$ and the measurement noise $v_k \sim (0, R_k)$ is white noise with covariance $R_k > 0$.

Between each measurement, the state estimate $\hat{z}_k$ and the estimation-error covariance matrix $P_k$ is propagated according to the known non-linear dynamics of the system:

$$\begin{aligned} \hat{z}_k^- &= f_{k-1}\left(\hat{z}_{k-1}^+, u_{k-1}, 0\right) \\ P_k^- &= T_{k-1} P_{k-1}^+ T_{k-1}^T + L_{k-1} Q_{k-1} L_{k-1}^T \end{aligned} \tag{28}$$

where $T_{k-1} = \frac{\partial f_{k-1}}{\partial z_{k-1}}\,|_{\hat{z}_{k-1}^+, u_{k-1}, 0}$ and $L_{k-1} = \frac{\partial f_{k-1}}{\partial w_{k-1}}\,|_{\hat{z}_{k-1}^+, u_{k-1}, 0}$. The state estimate and its covariance is updated through:

$$\begin{aligned} K_k &= P_k^- S_k^T \left(S_k P_k^- S_k^T + R_k\right)^{-1} \\ \hat{z}_k^+ &= \hat{z}_k^- + K_k\left[y_k - g_k\left(\hat{z}_k^-, u_k, 0\right)\right] \\ P_k^+ &= \left(I - K_k S_k\right) P_k^- \end{aligned} \tag{29}$$

where $S_k = \frac{\partial g_k}{\partial z_k}\,|_{\hat{z}_k^-, u_k, 0}$.

### 4.2. EKF implementation on correct medium tank plant data

The EKF algorithm was then applied to the correct medium tank system, using plant data. The filter was initialized at:

$$\boldsymbol{z}_{CM,0} = \begin{bmatrix} 1 & 0.017 & 0.017 & 3.4 & 0.02 \end{bmatrix}^T$$
$$\boldsymbol{P}_{CM,0} = \mathrm{diag}\begin{bmatrix} 1 & 0.1 & 0.1 & 10 & 0.1 \end{bmatrix}$$

The measurement noise covariance matrix $\boldsymbol{R}_{CM}$ is based on the noise seen in the instrumentation. The process noise covariance matrix $\boldsymbol{Q}_{CM}$ assumes equal uncertainty in $h_{lev(CM)}$, $Q_{CM}$, and $Q_{PD}$, while $\rho_{CM}$ and $Q_{in(CM)}$ are both assumed to have uncertainty one order of magnitude greater. $\boldsymbol{Q}_{CM}$ is also scaled according to the range of each process variable. Note that the EKF results are robust to different initialization values of $\boldsymbol{z}_{CM,0}$ and $\boldsymbol{P}_{CM,0}$, as well as to different values

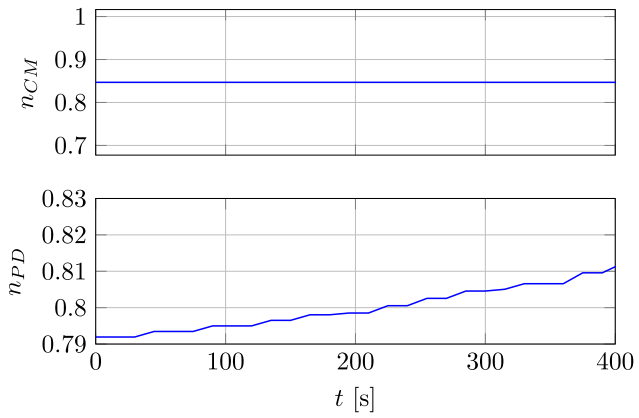


**Fig. 7.** Plant data of inputs to correct medium tank system.

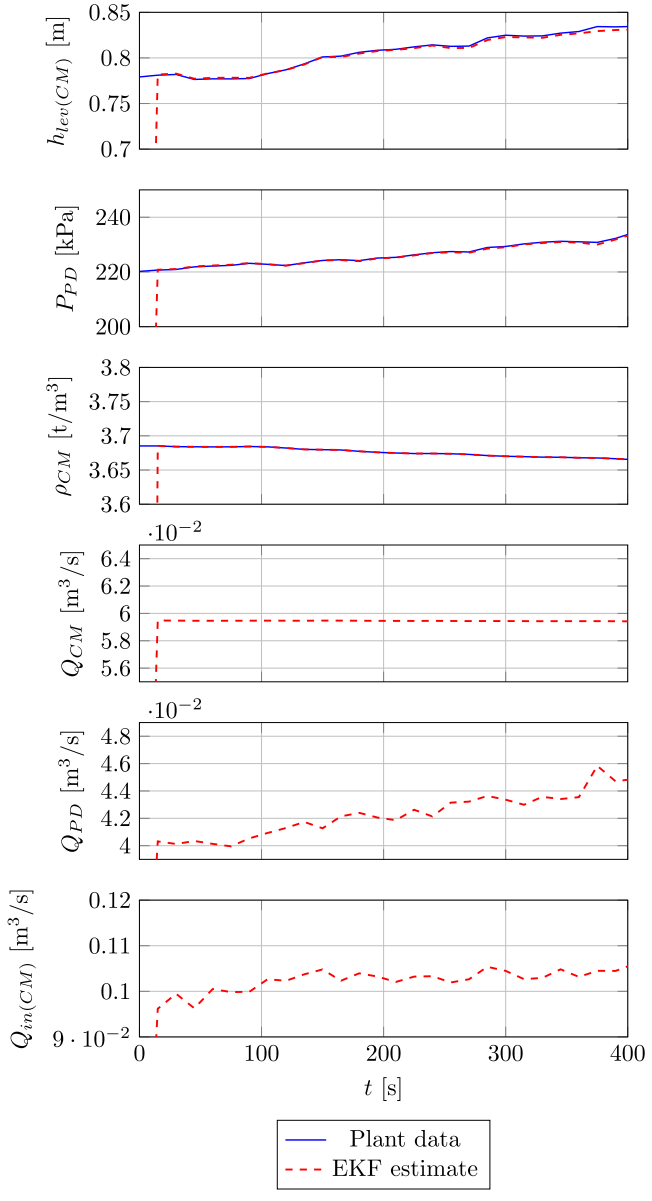


**Fig. 8.** Plant data and EKF estimates of correct medium tank system.

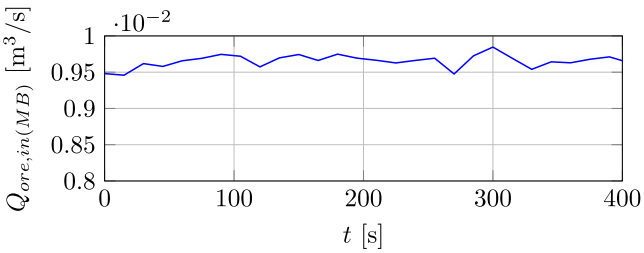


**Fig. 9.** Plant data of input to mixing box system.

of process noise covariance matrix $\boldsymbol{Q}_{CM}$, but are sensitive to changes of greater than 50% in the measurement covariance matrix $\boldsymbol{R}_{CM}$. (The EKF results for the mixing box, secondary tank and dilute medium tank described in Sections 4.3–4.5 respectively, are also similarly robust to different initialization values, different values of process noise covariance matrix, and sensitive to changes of greater than 20 to 50% in the measurement covariance matrix).

$$\boldsymbol{R}_{CM} = \text{diag}\begin{bmatrix}7.87\times10^{-4} & 0.0125 & 2.03\times10^{-6}\end{bmatrix}$$
$$\boldsymbol{Q}_{CM} = \text{diag}\begin{bmatrix}0.1 & 0.01 & 0.01 & 100 & 1\end{bmatrix}$$

The inputs to the system are given in Fig. 7. Fig. 8 shows plant data and the corresponding EKF estimates for the correct medium tank system outputs, as well as EKF estimates of the unmeasured model states. Note that the speed of the primary densifier pump, $n_{PD}$ in Fig. 7, is steadily increased in order to control the steadily increasing level of the correct medium tank, $h_{lev(CM)}$ in Fig. 8.

### 4.3. Extended Kalman filter implementation on mixing box plant data

The EKF algorithm was then applied to the mixing box system, using plant data. The filter was initialized at:

$$\boldsymbol{z}_{MB,0} = \begin{bmatrix}0.688 & 0.03 & 3 & 0.06\end{bmatrix}^T$$
$$\boldsymbol{P}_{MB,0} = \text{diag}\begin{bmatrix}1 & 0.1 & 10 & 0.1\end{bmatrix}$$

The measurement noise covariance matrix $\boldsymbol{R}_{MB}$ is based on the noise seen in the instrumentation. The process noise covariance matrix $\boldsymbol{Q}_{MB}$ assumes the uncertainty in $k_{MB}$, $\rho_{MB}$ and $Q_{CM}$ is one order of magnitude greater than that in $h_{lev(MB)}$. $\boldsymbol{Q}_{MB}$ is also scaled according to the range of each process variable.

$$\boldsymbol{R}_{MB} = \text{diag}\begin{bmatrix}0.027 & 1.122\times10^{-5} & 1.204\times10^{-4}\end{bmatrix}$$
$$\boldsymbol{Q}_{MB} = \text{diag}\begin{bmatrix}1 & 10 & 100 & 1\end{bmatrix}$$

Fig. 9 gives the input to the mixing box system during this period. Fig. 10 shows plant data and the corresponding EKF estimates for the mixing box system. Note that the flow of medium into the mixing box, $Q_{CM}$ in Fig. 10, while not measured in the plant, is an estimated state of the correct medium tank system.

In Fig. 10, from $t = 200$ s, the outlet pressure, $P_{MB}$ slowly increases, despite there being no increase in $Q_{CM}$ (see Fig. 8) or $Q_{ore,in(MB)}$ (see Fig. 9). This indicates a blockage, which is reflected in the state estimation of the mixing box level, $h_{lev(MB)}$ (see Fig. 10 at top), and in the estimation of the outlet coefficient $k_{MB}$ (in Fig. 10). The level increases steadily, while the outlet coefficient $k_{MB}$ decreases steadily, indicating a blockage. It is clear that no overflow occurred, as $h_{lev(MB)}$ remains below the maximum level of 1.5 m. It would be expected that, due to the blockage, the EKF state estimate of $Q_{in(CM)}$ seen in Fig. 8 would show a decrease, as the reason the mixing box level is increasing is because less material is flowing out of the mixing box and consequently, to the correct medium tank. However, this decrease is not apparent. This is because the reduction in flow out of the mixing box (and therefore in $Q_{in(CM)}$) is small in magnitude, and therefore not clear in the state estimation of $Q_{in(CM)}$ which contains some noise.

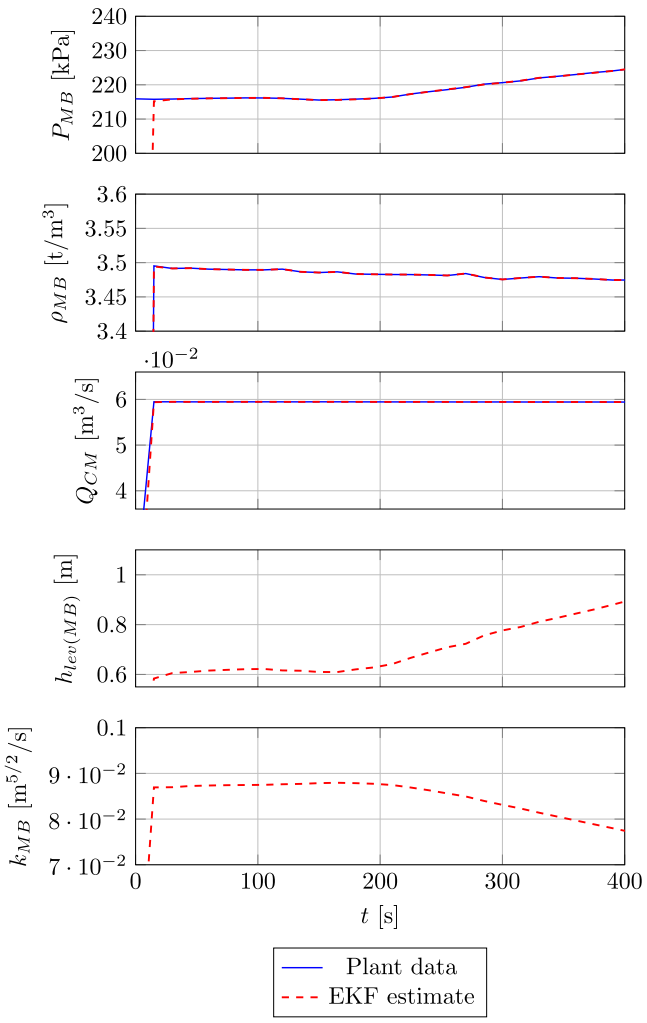


**Fig. 10.** Plant data and EKF estimates of mixing box system.

Despite not seeing the decrease in $Q_{in(CM)}$, the EKF estimate results, which show a clear decrease in $k_{MB}$ during the mixing box blockage (see Fig. 10), are significant as they demonstrate that a blockage in the mixing box, which could lead to an overflow and subsequent medium loss, can be detected.

### 4.4. EKF implementation on secondary tank plant data

The EKF algorithm was then applied to the secondary tank system, using plant data. The filter was initialized at:

$$\boldsymbol{z}_{sec,0} = \begin{bmatrix}0.825 & 0.017 & 3.4 & 0.02\end{bmatrix}^T$$
$$\boldsymbol{P}_{sec,0} = \text{diag}\begin{bmatrix}1 & 0.1 & 10 & 0.1\end{bmatrix}$$

The measurement noise covariance matrix $\boldsymbol{R}_{sec}$ is based on the noise seen in the instrumentation. The process noise covariance matrix $\boldsymbol{Q}_{sec}$ assumes equal uncertainty in $h_{lev(sec)}$ and $Q_{SD}$, while $\rho_{sec}$ and $Q_{in(sec)}$ are both assumed to have uncertainty one order of magnitude greater. $\boldsymbol{Q}_{sec}$ is also scaled according to the range of each process variable.

$$\boldsymbol{R}_{sec} = \text{diag}\begin{bmatrix}5.7\times10^{-3} & 1.94 & 2.15\times10^{-5}\end{bmatrix}$$
$$\boldsymbol{Q}_{sec} = \text{diag}\begin{bmatrix}0.1 & 0.01 & 100 & 1\end{bmatrix}$$

The input ($n_{SD}$, the speed of the secondary densifier pump) is given in Figs. 11, and 12 shows plant data and the corresponding EKF estimates for the secondary tank system outputs, as well as EKF estimates of the unmeasured model states.

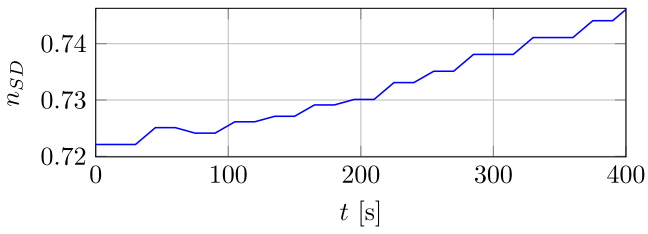


**Fig. 11.** Plant data of input to secondary tank system.

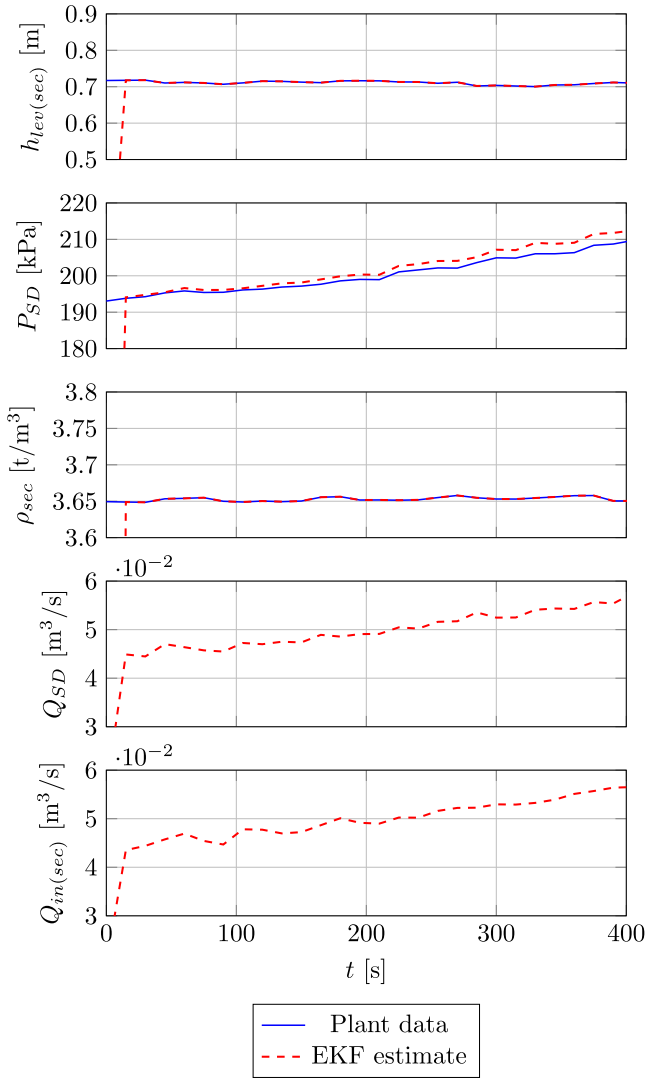


**Fig. 12.** Plant data and EKF estimates of secondary tank system.

As with $Q_{in(CM)}$, it is expected that a decrease in $Q_{in(sec)}$ is seen when the blockage in the mixing box at $t = 200$ s occurs. As with the state estimate of $Q_{in(CM)}$, this expected decrease is not visible in the EKF state estimate of $Q_{in(sec)}$ seen in Fig. 12. This is because the change in magnitude of $Q_{in(sec)}$ arising from the mixing box blockage is very small, considering that only a small fraction of the flow out of the mixing box reports to the secondary tank (with the bulk of this flow reporting to the correct medium tank). Instead, the estimate of $Q_{in(sec)}$ increases as $n_{PD}$ increases (see Fig. 7), as increasing $n_{PD}$ results in increasing flow to the primary densifier, and therefore to the secondary tank.

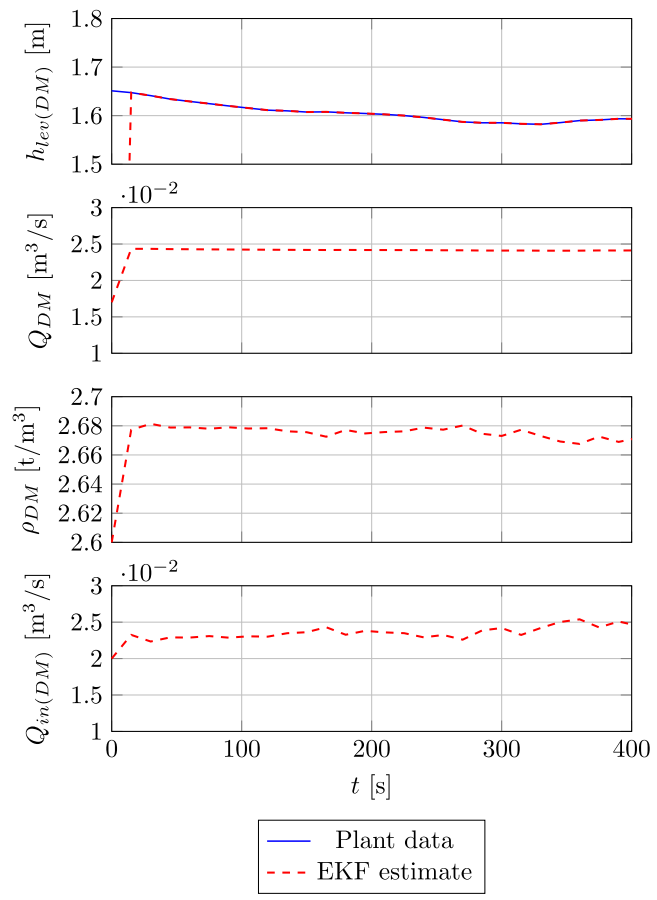


**Fig. 13.** Plant data and EKF estimates of dilute medium tank system.

### 4.5. EKF implementation on dilute medium tank plant data

The EKF algorithm was then applied to the dilute medium tank system, using plant data. The filter was initialized at:

$$\boldsymbol{z}_{DM,0} = \begin{bmatrix} 1 & 0.017 & 2.6 & 0.02 \end{bmatrix}^T$$
$$\boldsymbol{P}_{DM,0} = \text{diag}\begin{bmatrix} 1 & 0.1 & 10 & 0.1 \end{bmatrix}$$

The measurement noise covariance matrix $\boldsymbol{R}_{DM}$ is based on the noise seen in the instrumentation. The process noise covariance matrix $\boldsymbol{Q}_{DM}$ assumes equal uncertainty in $h_{lev(DM)}$ and $Q_{DM}$, while $\rho_{DM}$ and $Q_{in(DM)}$ are both assumed to have uncertainty one order of magnitude greater. $\boldsymbol{Q}_{DM}$ is also scaled according to the range of each process variable.

$$\boldsymbol{R}_{DM} = \text{diag}\left[8.57 \times 10^{-5}\right]$$
$$\boldsymbol{Q}_{DM} = \text{diag}\begin{bmatrix} 0.1 & 0.01 & 100 & 1 \end{bmatrix}$$

Since the dilute medium pump is a fixed speed pump, $n_{DM} = 1$ throughout the estimation period. The results of the EKF implementation on the system outputs and states can be seen in Fig. 13.

### 4.6. State estimation for medium loss detection

Section 4 has shown that the key variables in the circuit in which the effect of medium losses is seen (namely $Q_{in,(CM)}$, $Q_{in,(sec)}$, $k_{MB}$ and $h_{lev(MB)}$) can be effectively estimated using an EKF. It is clear that losses due to overflow of the mixing box can be detected as $k_{MB}$ and $h_{lev(MB)}$ are effectively estimated (see Fig. 10). Furthermore, the response seen in these variables due to a blockage ($k_{MB}$ decreases and $h_{lev(MB)}$ increases) is unique to this situation, and cannot be caused by another disturbance. Whether a blockage is causing overflow (and consequently medium losses), can be confirmed by checking if the estimate of $h_{lev(MB)}$ exceeds the maximum mixing box level, and by checking if the state estimate of $Q_{in(CM)}$ shows an unexpected decrease (ie., a decrease that cannot be explained by a decrease in $n_{CM}$).

However, in the case of the screen losses and the magnetic separator losses, a change in the split of the primary or secondary densifiers could produce the same effect on $Q_{in,(CM)}$ and $Q_{in,(sec)}$ as would be expected from these losses. It is therefore not possible to definitively identify these losses when they occur. Installing a flow meter on the overflow of the secondary densifier can resolve this issue, and allow for these losses to be detected.

## 5. Conclusion and recommendations

A model for the flow of medium through a dense medium separation circuit has been developed. The observability of the unit models was analysed, including that of adapted unit models which assume that some disturbance variables and parameters in the models, not available for measurement, are unknown. The models of the primary and secondary densifiers, the magnetic separator, and the combined dense medium cyclone and drain-and-rinse screen systems are not instrumented, and therefore cannot be verified online. However, the correct medium, secondary and dilute medium tank systems were shown to be fully observable, including for the case where the flow rate of medium into these tanks is assumed unknown (a necessary assumption given the lack of instrumentation on the drain-and-rinse screens, primary and secondary densifiers, and magnetic separator). Additionally, the mixing box system was shown to be fully observable, including for the case where the value of the constant $k_{MB}$ is not known.

An EKF was designed for state estimation of the fully observable units — the correct medium, secondary, and dilute medium tank systems, and the mixing box system. Plant data for a mixing box blockage is available, and so the EKF was applied to this data and could estimate all the states of the observable units. The state estimation illustrated that the mixing box blockage can be seen in the EKF estimate of the mixing box states: $h_{lev(MB)}$ increases without any increase in the flow of ore or medium into the mixing box, and $k_{MB}$ decreases.

An analysis of the three key sources of medium loss indicated that medium losses can be detected in their effect on key circuit variables: $Q_{in(CM)}$, $Q_{in(sec)}$, $h_{lev(MB)}$, and $k_{MB}$. The observability analysis showed that these variables are all observable. However, only a mixing box blockage causes a unique effect in observable variables. Medium losses at the drain-and-rinse screens, and losses to the magnetic separator, cause an effect on the circuit that could be caused by other unmeasured disturbances (such as a change in the split of the secondary densifier). Therefore, only medium losses due to overflow at the mixing box can be definitively identified. The state estimation developed here can be integrated with the live plant data to detect mixing box blockages in real time, thus enabling reduction of medium losses due to mixing box overflows and reducing operating costs for the plant. Further instrumentation will be required to detect the remaining sources of loss.

It should be noted that the approach for assessing medium losses taken in this paper is qualitative. Fault detection and isolation using model-based fault detection (Jung and Sundstrom, 2019) can be applied to this problem in future work to provide a quantitative method.

## CRediT authorship contribution statement

**C.S. Lowry:** Conceptualization, Data curation, Investigation, Resources, Software, Writing – original draft. **J.D. le Roux:** Funding acquisition, Project administration, Supervision, Validation, Writing – review & editing. **I.K. Craig:** Supervision, Validation, Writing – review & editing.

## Declaration of competing interest

Johan Derik le Roux was provided by National Research Foundation of South Africa. If there are other authors, they declare that they have no known competing financial interests or personal relationships that could have appeared to influence the work reported in this paper.

## Data availability

The data that has been used is confidential.

## Acknowledgment

This work is based on the research supported in part by the National Research Foundation of South Africa (Grant Numbers: 137769).

## Appendix

### *Dense medium cyclone and drain-and-rinse screens*

For the purposes of modelling the flow of medium through the DMS circuit, the dense medium cyclone and drain-and-rinse screens, shown in Fig. 1, is simplified as shown in Fig. 14. Therefore, the flow of medium from the DMC and screens is modelled as follows:

$$Q_{drain}(t) = k_{DMC} Q_{in(DMC)}(t - \tau_{DMC}), \tag{30}$$

for $t > \tau_{DMC}$, where $Q_{drain}$ [m$^3$/s] is the flow of medium out of the unit to the correct medium tank, $Q_{in(DMC)}$ [m$^3$/s] is the flow of medium out of the mixing box (obtained from the flow of medium and ore out of the mixing box, assuming the same ore-to-medium ratio in the mixing box discharge as that of the mixing box feed) to the dense medium cyclone, and $\tau_{DMC}$ [s] is the delay term. The inclusion of the parameter $k_{DMC}$ is to accommodate any instances where the flow of medium out of the system might differ from the flow into the system. This can be used to model instances of medium losses at the drain-and-rinse screens.

### *Densifiers*

The primary densifier is a battery of six hydrocyclones fed from the primary densifier pump. The hydrocyclones separate feed based on density into the overflow (lower density) and underflow (higher density). For this work, a steady-state model of the volumetric split is used, as the dynamics of this unit process are assumed fast. The volumetric split of a single hydrocyclone is given by (Flintoff et al., 1987; Bueno, 2021):

$$S_{cyc} = \frac{Q_{UF}}{Q_{OF}} = k_{cyc} h_{cyc}^{0.19} \left( \frac{d_{apex}}{d_{vortex}} \right)^{2.64} \frac{e^{-4.33\alpha + 8.77\alpha^2}}{P_{feed}^{0.54} d_{cyc}^{0.38}} \tag{31}$$

where $d_{apex}$ [mm] is the diameter of the cyclone apex, $d_{vortex}$ [mm] is the diameter of the cyclone vortex, $d_{cyc}$ [mm] is the diameter of the cyclone, $h_{cyc}$ [mm] is the height of the cyclone, $\alpha$ is the solids fraction in the feed, per volume unit, $P_{feed}$ [kPa] is the feed pressure to the hydrocyclone, and $Q_{UF}$ [m$^3$/s] and $Q_{OF}$ [m$^3$/s] is the cyclone under- and overflow respectively. The parameter $k_{cyc}$ is a fitting parameter (Sepúlveda, 2004). Table A.10 gives the values of the parameters for (31).

Because the primary densifier consists of a battery of six hydroclones, the overall volume split $S_{PD}$ is assumed to be equal to the individual volumetric split $S_{cyc}$ of a single hydrocyclone. The underflow and overflow of the primary densifier can be modelled as follows:

$$Q_{OF(PD)} = \frac{Q_{feed(PD)}}{S_{PD} + 1}, \tag{32}$$

where $Q_{OF(PD)}$ [m$^3$/s] is the volumetric flow rate of the primary densifier overflow (which reports to the secondary tank), and $Q_{feed(PD)}$ [m$^3$/s] is the volumetric flow rate of the primary densifier feed.

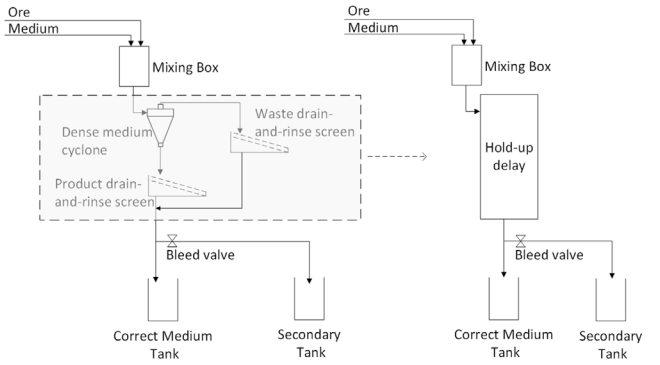


**Fig. 14.** Diagram showing model simplification of the dense medium cyclone and drain-and-rinse screens. Only the drained medium flow is shown. The flow of rinsed medium, which reports to the dilute medium tank, is not depicted, and considered negligible.

**Table A.10**
Primary densifier parameters.

| Variable | Value | Description |
|---|---|---|
| $d_{apex}$ | 45 mm | Hydrocyclone apex |
| $d_{vortex}$ | 70 mm | Hydrocyclone vortex |
| $d_{cyc}$ | 165 mm | Hydrocyclone diameter |
| $h_{cyc}$ | 350 mm | Hydrocyclone height |
| $k_{cyc}$ | 54.96 | Hydrocyclone fitting coefficient |

The secondary densifier, in contrast to the primary densifier, is a pipe densifier. This type of densifier is not well explored in the literature. Legault-Seguin et al. (2017) gives typical mass balance values for a pipe densifier found in a dense medium separation circuit, and so for this work these typical values will be used. Therefore, the volumetric split of the secondary densifier is assumed to be $S_{SD} = 2.3$ such that:

$$Q_{OF(SD)} = \frac{Q_{feed(SD)}}{S_{SD} + 1} = \frac{Q_{feed(SD)}}{3.3}, \tag{33}$$

where $Q_{OF(SD)}$ [m$^3$/s] is the volumetric flow rate of the secondary densifier overflow (which reports to the dilute medium tank), and $Q_{feed(SD)}$ [m$^3$/s] is the volumetric flow rate of the secondary densifier feed.

### *Magnetic separator*

The magnetic separator is modelled in steady-state, as the dynamics of the volumetric split between the concentrate and the effluent outputs of the magnetic separator are considered much faster than the rest of the circuit. The magnetic separator is modelled according to Rayner and Napier-Munn (2003a), in which a mathematical model of the concentrate solids content for a wet drum magnetic separator was developed. The concentrate flow $Q_D$ [m$^3$/h] is modelled as:

$$Q_D = k_1 Q_f \left( \frac{D^2 \omega}{Q_f} \right)^{k_2} \left( \frac{x_p}{D} \right)^{k_3} \left( \frac{x_d}{D} \right)^{k_4} \alpha_f^{k_5} \left( \frac{\rho_s Q_f}{M_f} \right)^{k_6}, \tag{34}$$

where $k_1$, $k_2$, $k_3$, $k_4$, $k_5$, $k_6$ are parameters to be fitted, $D$ [m] is the drum diameter, $\omega$ [rad/s] is the drum rotational velocity, $x_p$ [m] and $x_d$ [m] are the pickup and discharge gaps respectively, $\alpha_f$ is the feed moisture, $Q_f$ [m$^3$/h/m] and $M_f$ [t/h/m] are the volumetric and mass feed rates per unit length respectively, and $\rho_s$ [t/m$^3$] is the solids density.

The magnetic separator in operation at the DMS plant is not well instrumented. The feed density and flow are not measured, and neither are the drainage flow rate or density. Fitting the parameters in (34) is therefore impractical, and not the focus of this work. For the purposes of this work, (34) is simplified as follows:

$$Q_{MS} = Q_{feed(MS)} k_{MS}, \tag{35}$$

where $Q_{MS}$ [$m^3$/s] is the flow rate of concentrate from the magnetic separator to the correct medium tank, $Q_{feed(MS)}$ [$m^3$/s] is the feed flow rate to the magnetic separator, and $k_{MS}$ is given a nominal value of 0.048 (obtained from mass balances of magnetic separators given in Legault-Seguin et al. (2017)). In future work, this value can be changed in order to simulate medium losses to the magnetic separator effluent, which are generally significant contributors to medium losses (Dardis, 1989).

## References


Bueno, E.A., 2021. Simulacao De Hidrociclones (Ph.D. thesis). Universidade Federal de Ouro Preto.

Dardis, K.A., 1989. The design and operation of heavy medium recovery circuits for improved medium recovery. Coal Prep. 7 (3–4), 119–157.

Flintoff, B.C., Plitt, L.R., Turak, A.A., 1987. Cyclone modelling: a review of present technology. CIM Bull. 80, 39–50.

Ghafouri, J.H., Khayatzadeh, F.H., Khayatzadeh, A.H., 2012. Dynamic modeling of variable speed centrifugal pump utilizing MATLAB/Simulink. Int. J. Sci. Eng. Invest. 1 (5).

Jang, L.K., 2016. Level control by regulating control valve at the bottom of a gravity-drained tank. Chem. Eng. Educ. 50 (4), 245–250.

Jung, D., Sundstrom, C., 2019. A combined data-driven and model-based residual selection algorithm for fault detection and isolation. IEEE Trans. Control Syst. Technol. 27 (2), 616–630.

Kallesoe, C., Cocquempot, V., Izadi-Zamanabadi, R., 2006. Model based fault detection in a centrifugal pump application. IEEE Trans. Control Syst. Technol. 14 (2), 204–215.

Karassik, I.J., 2008. Centrifugal pump theory, analysis, and performance. In: Pump Handbook. McGraw-Hill Professional, pp. 29–117.

Legault-Seguin, E., Mohns, C., Rylatt, M., 2017. Dense medium separation: An effective and robust preconcentration technology. CIM J. 8 (3), 244.

Maré, E., Beven, B., Crisafio, C., 2015. 10 - Developments in nonmagnetic physical separation technologies for hematitic/goethitic iron ore. In: Lu, L. (Ed.), Iron Ore. Woodhead Publishing, pp. 309–338.

Meyer, E.J., Craig, I.K., 2010. The development of dynamic models for a dense medium separation circuit in coal beneficiation. Min. Eng. 23 (10), 791–805.

Minerals, W., 2012. Warman centrifugal slurry pumps. URL http://web.archive.org/web/20080207010024/http://www.808multimedia.com/winnt/kernel.htm, (accessed 2023-09-30).

Napier-Munn, T., 2018. The dense medium cyclone–past, present and future. Min. Eng. 116, 107–113.

Napier-Munn, T.J., Kojovic, T., Scott, I.A., Shi, F., Masinja, J.H., Baguley, P.J., 1995. Some causes of medium loss in dense medium plants. Min. Eng. 8 (6), 659–678.

Rayner, J.G., Napier-Munn, T.J., 2003a. A mathematical model of concentrate solids content for the wet drum magnetic separator. Int. J. Miner. Process. 70 (1–4), 53–65.

Rayner, J.G., Napier-Munn, T., 2003b. A mathematical model of recovery of dense medium magnetics in the wet drum magnetic separator. Int. J. Miner. Process. 69 (1), 157–173.

Schneider, R., Georgakis, C., 2013. How to not make the extended Kalman filter fail. Ind. Eng. Chem. Res. 52 (9), 3354–3362.

Scott, N.J.C., 2017. Dynamic Analysis of Dense Medium Circuits (Ph.D. thesis). The University of Queensland.

Seborg, D.E., Edgar, T.F., Mellichamp, D.A., Doyle III, F.J., 2016. Process Dynamics and Control. John Wiley & Sons.

Sepúlveda, J.E., 2004. Methodologies for the evaluation of grinding media consumption rates at full plant scale. Min. Eng. 17 (11–12), 1269–1279.

Simon, D., 2006. Optimal State Estimation: Kalman, H Infinity, and Nonlinear Approaches. John Wiley & Sons.

Skogestad, S., Postlethwaite, I., 2005. Multivariable Feedback Control: Analysis and Design. Wiley.

Tom, P., 2015. Optimization of Dense Medium Cyclone Plant for the Beneficiation of Low Grade Iron Ore with Associated High Proportion of Near-Density Material at Sishen Iron Ore Mine (Ph.D. thesis). University of the Witwatersrand.

Versteeg, H.K., Malalasekera, W., 2007. Conservation laws of fluid motion. In: An Introduction To Computational Fluid Dynamics, second ed. Pearson, pp. 9–17.